HHS Public Access

Author manuscript

Semin Roentgenol. Author manuscript; available in PMC 2017 October 01.

Published in final edited form as:

Semin Roentgenol. 2016 October ; 51(4): 308–316. doi:10.1053/j.ro.2016.05.015.

MR imaging of the liver (including biliary contrast agents):

Part 1: technical considerations and Contrast Materials

A Agostini[1,2], **MF Kircher**[1], **R Do**[1], **A Borgheresi**[1,3], **S Monti**[4], **A Giovagnoni**[2], and **L Mannelli**[1]

[1]Department of Radiology, Memorial Sloan-Kettering Cancer Center, 1275 York Avenue, New York, NY 10065

[2]School of Radiology, Universita' Politecnica delle Marche, Via Tronto 10, 60126 Ancona, Italy

[3]School of Radiology, Universita' degli Studi di Firenze, Largo Brambilla 3, 50134 Firenze, Italy

[4]IRCCS SDN, Via Emanuele Gianturco 113, 80143 Napoli, Italy

Introduction

Magnetic Resonance Imaging (MRI) plays a key role in the non-invasive evaluation of liver pathologies, because it is capable of providing comprehensive and highly accurate diagnostic information, with the additional advantage of lack of harmful ionizing radiation.

The aim of this review is to provide the essential information to implement a basic MR protocol of liver. Major advances in MRI technology have been achieved in the last decade regarding 1) hardware (high-performance gradient coils and phased-array surface coils), 2) software (new sequences; new parallel imaging technology and other acceleration techniques), and 3) contrast media (CM), and have made a major impact on MRI of the liver. The study of the liver presents several technical issues in particular due to the anatomical position and the mobility with the respiration. In the following sections we will discuss about the principal technical challenges and solutions available for the study of the liver, such the MRI study at high field strengths, the use of parallel imaging, and the control of motion-related artifacts. In the last section we will provide the principal information for the use of contrast materials.

Liver MRI: Technical considerations

B_0 field strength: 1.5T and 3T—Most of the standard liver protocols are implemented on 1.5T magnets. Imaging at higher field strengths, such at 3T, is finding more widespread use with the promise of several benefits [1].

Corresponding authors: Andrea Agostini, MD, Department of Radiology, Memorial Sloan Kettering Cancer Center, 1275 York Avenue, New York NY 10065, School of Radiology, Universita' Politecnica delle Marche, Via Tronto 10, 60126 Ancona, Italy, dott.andrea.agostini@gmail.com. Lorenzo Mannelli, MD, PhD, Department of Radiology, Memorial Sloan Kettering Cancer Center, 1275 York Avenue, New York NY 10065, mannelll@mskcc.org.

The main advantage of imaging at 3T in comparison with 1.5T is in the larger number of excitable protons, proportional to the static magnetic field B_0; these additional excited protons can be used to improve image quality or to shorten acquisition time. At 3T, the signal-to-noise ratio (SNR) is expected to increase since the signal is proportional to B_0^2, while the intrinsic noise is proportional to B_0. This implies that in a perfect system the SNR of a 3.0T system is twice as higher than that of a 1.5T system. In practice, however, this improvement in SNR is not fully achieved due to the influence of other parameters such as voxel volume, phase encoding steps, number of partitions, number of excitations, changes in relaxation times (mainly T1), and the effect of the flip angle in gradient echo sequences [2].

The improvement of SNR at 3T is limited by the specific absorption rate (SAR), which is proportional to B_0^2. The most affected pulse sequences are the fast spin echo (FSE) and gradient echo (GRE). Reduction of flip angle and number of slices, and increase of repetition time (TR) may represent a solution to keep SAR within the allowed limits [1, 3]. Other techniques such as variable refocusing flip angles or variable-rate selective excitation have been developed to reduce energy deposition [4, 5].

The precession frequency of water protons is proportional to B_0 and increases from ~64 MHz at 1.5T to ~128 MHz at 3T. This results in lower efficiency of energy transfer with consequent longer T1 relaxation times at 3T. The increments of T1 relaxation time are not uniform in different soft tissues. T1 relaxation times increase substantially for bound water, slightly for adipose tissue, and remain near constant for free water. In contrast to T1 relaxation times, T2 relaxation times are not significantly affected by differences in field strength [6, 7]. T2 weighted sequences at 3T provide higher fluid signal and better lesion conspicuity, in particular in magnetic resonance cholangiography (MRCP) [8].

Compared to 1.5T, the relaxivity of CM decreases approximately 5–10% (table I), but this is compensated by the increase in T1 relaxation times of soft tissues resulting in an overall higher contrast-to-noise ratio (CNR) at 3T [9].

Some artifacts are exacerbated and new specific artifacts can be encountered at 3T. Chemical shift artifact is caused by the difference in resonance frequencies between water and fat protons, which increases from ~225 Hz at 1.5T to ~450 Hz at 3T. In particular, the India ink artifact due to spatial misregistration will appear twice as wide on the 3T images; this can be reduced by using fat suppression or increasing the receiver bandwidth; however, increasing the bandwidth would result in a loss in the SNR [10]. Conductivity and permittivity properties of water present in soft tissues are responsible of B_1 inhomogeneity artifacts. The resulting standing waves and shielding artifacts cause abnormal signal loss visible as hypointense areas within the image [3]. A possible solution to these artifacts consists in RF cushions positioned on the patient’s abdominal wall. These usually consist of high water content gel mixed with high concentration of Gd-based CM to disrupt the wave interferences within the abdomen and the cushion itself [11].

Susceptibility artifacts are intensified at 3T. They are caused by variations in the local magnetic field homogeneity, presence of metal or the interface of two materials with different magnetic susceptibilities (e.g. air-tissue), leading to T2* dephasing. This can be of

some advantage for detection of unphysiologic air bubbles (e.g. pneumobilia), but is most of the time detrimental to image quality. The sequences most sensitive to susceptibility artifacts are gradient echo (GRE), echo planar (EPI), and inversion recovery (IR) [3].

Banding artifacts in balanced steady-state free precession GRE (BSSFP) may increase at higher magnetic fields. Possible solutions are decreasing the voxel size, optimizing B_0 shimming, and using shorter echo times and increased bandwidth for GRE sequences, parallel imaging for EPI, and a shorter TR for BSSFP [3].

Medical devices safe for use in 1.5T magnets are not necessarily safe at 3T, and, finally, the installation and maintenance of a 3T magnet are more expensive than 1.5T [10].

Parallel imaging—In parallel imaging (PI), k-space is under-sampled along the phase-encoding direction while using multiple parallel receiving coils (or array coils with multiple elements). Each coil element works independently and has spatial sensitivity for a specific portion of the field of view (FOV) [12]. K-space is under-sampled by an acceleration factor *r*, which can theoretically reach the number of coil elements minus 1. Specific algorithms provide the missing spatial information of the acquired field-of-view (FOV) by analyzing spatial sensitivity of coil elements [12, 13].

Algorithms for PI can operate in the image domain or k-space domain:

- Algorithms operating in the image domain: *Sensitivity Encoding* (SENSE) and *array spatial sensitivity encoding technique* (ASSET). The information about spatial sensitivity of coil elements is provided by the calibration performed before image acquisition. After image reconstruction, the algorithm unfolds and weights each pixel by the spatial sensitivity of the coil elements [14].
- Methods operating in the k-space domain. *Generalized auto-calibrating partially parallel acquisition* (GRAPPA) is derived from *simultaneous acquisition of spatial harmonics* (SMASH) techniques, in particular from AUTO-SMASH and variable-density AUTO-SMASH (VD-AUTO-SMASH) [15–18]. These techniques are based on the principle that spatial sensitivity of an array coil is a sinusoidal function, used to obtain spatial information (spatial harmonics). The spatial sensitivity map is obtained by acquiring few more k-space lines during imaging acquisition (auto-calibration) [18].

Further evolution is represented by volumetric techniques and multislice acquisitions. As an example, *controlled aliasing in parallel imaging results in higher accelerations* (CAIPIRINHA) uses a multiband RF pulse for the excitation of multiple slices that are undersampled [19].

Two parameters of PI algorithms influence image quality: The acceleration factor *r* (defined above), and the geometrical factor *g* dependent on coil design (elements and configuration) indicating the noise amplification in image reconstruction. In general, SNR is inversely proportional to g and $\sqrt{r}$ [12, 13]. In general, eight channel array coils are required for liver imaging at 1.5-3T and a *r* factor of 2–3 usually provides images of good quality with most sequences [12].

The first and obvious advantage is the shorter acquisition time, useful to reduce motion artifacts and for breath-hold sequences in uncooperative patients. At constant acquisition time, PI provides better spatial resolution and wider anatomical coverage; PI can also be implemented to improve both spatial and temporal resolution [13, 20].

Technical limits of imaging at 3T take benefit of PI techniques. The under-sampling of k-space leads to lower energy deposition with lower SAR, useful in GRE sequences (in particular steady state sequences, SSFP). PI can improve blurring artifacts of single shot fast spin echo with half-Fourier acquisition sequence (SSFSE) by allowing shorter echo trains [20].

Motion related artifacts and technical solutions—Most of MR pulse sequences require longer acquisition times compared to physiological movements such a cardiac, breathing, and bowel motion: this causes blurring and ghosting artifacts [21]. In liver imaging, respiration is the most important source of artifacts.

Motion artifacts occur along the phase encoding direction when the movement period is of the same order of the time passing between subsequent phase encoding steps [22].

The solutions available to overcome motion artifacts can be classified in three groups: 1) motion elimination or reduction, 2) artifact reduction, and 3) motion correction [22].

Motion elimination or reduction: The easiest solution to motion artifacts is the suppression (or reduction) of the movement, such as breath-holding for respiratory artifacts, administration of smooth muscle relaxants for peristalsis, or cough suppressants for cough.

Breath-hold techniques are commonly used in liver imaging. Breath-holding requires patient education and collaboration during image acquisition. Unfortunately some subjects are unable to suspend their respiration.

A healthy human at rest has a respiratory cycle of 4–5 seconds (s) with 14–16 cycles per minute (min): inspiration and expiration phases last nearly 2 s, and there is a pause of ~1s at the end of expiration. A healthy subject achieves an average breath-hold apnea of 20–30s; this is slightly longer after a deep inspiration. Some patients may not be able to achieve such long breath-holding times. In deep respiration, the diaphragmatic position is more reproducible at the end of the expiratory phase: breath-hold acquisitions are preferred in this phase in spite of shorter achievable apnea in expiration compared to inspiration [23, 24].

In case of breath-held acquisitions longer than the apnea time, the sequence can be split in two or more parts. A downside of this solution is a possible incomplete anatomical coverage due to possible inconsistent positions of the diaphragm between different breath-holds. A solution to this potential inconvenience is planning some overlap between the split volumes [25].

Changing the phase encoding direction may improve the unwanted effects of motion artifacts that then appear in a different position. This is an easy solution to solve this kind of artifacts if detected while the patient is still in the scanner, and requires additional time.

Artifact Reduction

Respiratory gating and triggering: Respiration can be approximated to a periodic movement, represented as a waveform which can be studied by placing respiratory bellows on the patient's thoracic or abdominal wall. Image acquisition can be synchronized to the respiratory activity with two methods:

- Respiratory gating. It consists in data collection only within a temporal window of the respiratory cycle; the temporal window is defined by opening and closing points set along the respiratory wave. The acquisition window is chosen at the end of the expiratory phase for two reasons: at the end of expiration the position of diaphragm has a lower variability and it remains still for a longer time [24].
- Respiratory triggering. It consists of starting the data collection at a precise point of the respiratory wave. The trigger point opening the acquisition window can be set at any time of the respiratory wave and the acquisition lasts a fixed time without the need of a closing point. The respiratory triggering results in shorter acquisition times in comparison with gating, but it is prone to artifacts due to inconsistency of breathing motions [24, 26]. Moreover, at our institution, the trigger point and the window length is adjusted on the type of breath, as an example: steady breath (trigger point 30%, window 31%), deep breath (trigger point 20%, window 21%), and shallow breath (trigger point 10%, window 11%).

These techniques may be associated to phase reordering techniques, which change the filling order of k-space lines in relation to the respiratory waveform. As an example, close k-space lines are filled at the same point of the respiratory cycle (ROPE: respiratory ordered phase encoding) [27].

Respiratory gating and triggering require less patient collaboration, and a regular respiratory activity optimize the acquisition times.

Cardiac gating: The monitoring of cardiac activity is rarely required in liver imaging. The evaluation of a small liver lesion in the left lobe, close to the heart, may require cardiac gating. This can be obtained by placing electrocardiographic (ECG) electrodes on the chest wall of the patient, or using a finger pulse oximeter. ECG gating associated with respiratory gating is feasible but results in long acquisition times [22].

Faster sequences and optimization of k-space filling: Following an analogy with photography, an intrinsic solution to motion artifacts is filling the k-space in a time shorter than the period of motion frequency; PI can help to reduce acquisition times [20]. BSSFP, SPGR and SSFSE are fast sequences that can sample the k-space in a fraction of a second, which is shorter than the period of motion frequency of the respiratory cycle [28, 29]. EPI sequence fills the entire k-space within a repetition time (TR) and is routinely used in liver diffusion weighted imaging (DWI). The drawbacks of rapid acquisitions usually are a lower spatial resolution, a loss in lesion-to-liver CNR, and blurring artifacts due to long echo trains [29]. BSSFP sequence provides images with high SNR, but the signal weighting is dependent on T2/T1, limiting its application for liver lesion detection and characterization [30].

Motion artifacts affect mostly the central region of the k-space because of the lower spatial frequency. Techniques like *periodically rotated overlapping parallel lines with enhanced reconstruction* (PROPELLER) optimize the k-space filling by oversampling the central region with reduction of motion artifacts [31, 32].

Motion correction: Navigators: Navigators are algorithms that obtain information about the moving structures from short RF pulses (navigator echoes) included in the imaging sequence, without external devices. Depending on the design of the navigator, they can detect movements up to the three dimensions in space, with increasing complexity [24, 33]. In liver imaging, mono- or bidimensional navigators are preferred because of the diaphragmatic kinetics and lower complexity of algorithms. The volume to be sampled is a cylinder or a slice (e.g. coronal). It is positioned with its center tangent to the right hemidiaphragm because of the high signal contrast between liver and lung. The diaphragm position is detected in relation to a reference image or with edge-detection algorithms (figure 1).

Navigators require a high temporal resolution without interference with liver proton magnetization. Usually fast spoiled gradient echo (FLASH) sequences are preferred. The low flip angle (i.e. 10°) gives a good contrast without significant interference with the magnetization of the liver tissue included in the volume of interest [34, 35]. Navigators allow for implementing gated and triggered techniques [34, 36, 37].

Contrast materials—Magnetic Resonance provides images with intrinsic high tissue contrast; however, this is often not sufficient to detect and characterize focal liver lesions. Normal liver parenchyma has a characteristic double vascularization through the hepatic artery and portal vein. The injection of a contrast material (CM) enables detecting and characterizing focal lesions exploiting differences in perfusion between liver parenchyma and focal liver lesions, as well as perfusion differences among different focal lesions. Moreover, hepatospecific contrast agents add functional information to vascular findings.

Most of the CM used in liver imaging are based on paramagnetic properties of gadolinium (Gd), while superparamagnetic CM (iron oxides) are not routinely used in standard liver protocols. Manganese is a superparamagnetic element, not discussed in this review since it is not commercially available. In the next sections, CM will be divided in paramagnetic and superparamagnetic, the formers divided in relation to the different pharmacokinetic properties due to the chemical structure of chelating compound.

Paramagnetic CM: Gadolinium

Pharmacodynamics: The lanthanide ion Gd^{3+} has a spin of 7/2 with seven external unpaired electrons that are responsible of paramagnetic properties. The interactions between external electrons of Gd^{3+} and water protons are complex and result in shortening of T1 and T2 relaxation times [38]. In the basic liver protocols, paramagnetic CM are used to enhance T1 signal [39].

Chemistry of chelating compounds: The toxicity of Gd^{3+} requires chelation before administration in human beings [40]. The chemical structure of the chelating compound has

important influences on pharmacokinetics (excretion), pharmacodynamics (relaxivity), and safety profile (e.g. nephrogenic systemic fibrosis, NSF) [41].

The Food and Drug Administration (FDA) has approved 9 Gd-based CM for clinical use [42–50]. The chemical structure of the chelating compounds classifies the Gd-CM in linear and macrocyclic, further divided in ionic and non-ionic (table I). This classification is relevant because the different molecular structure of chelating compounds have influence on Gd^{3+} dissociation [39, 51]. Stability of Gd-compounds can be defined as the energy necessary to dissociate Gd^{3+} from the chelating compound or the rate at which Gd^{3+} dissociates from its chelating compound. This concept can be expressed with the more intuitive parameter of dissociation half-life ($T_d1/2$, see table I), which increases as the stability constants increase [52, 53]. This is an important aspect because free Gd^{3+} is deemed one of the pathophysiological factors of NSF: macrocyclic and ionic compounds have higher stability than linear or non-ionic complexes, and the European Society of Urogenital Radiology (ESUR) uses this rationale for guidelines for contrast administration in subjects at risk for NSF (table I) [41, 54]. Table I also compares the classification of paramagnetic contrast materials provided by the American College of Radiology (ACR) regarding the risk of NSF [55]. As a difference with the ESUR Guidelines, the classification of ACR uses epidemiological criteria: the group 1 contains the molecules mostly related to NSF and corresponds to ESUR High Risk group (table I). The lack of overlap among ACR groups 2 and 3 with ESUR Intermediate and Low risk groups is due mostly to the commercialization of different molecules in different periods [41, 55].

The addition of specific moieties to the chelating complexes is responsible for binding to proteins: this results in differences in pharmacokinetics (different clearance and different elimination half-life) as well as in pharmacodynamics (higher relaxivity), as shown in table I [9, 39, 42–50, 56]. MS-325 has high affinity for plasma proteins resulting in low diffusion in the interstitium and low renal excretion and long elimination half-life (table I) [45]. Gd-BOPTA and Gd-EOB-DTPA (hepatospecific CM) weakly bind albumin and have partial hepatocellular active uptake [43, 44]. The other Gd-based CM (extracellular/interstitial CM) are designed not to bind to plasma proteins; these CM diffuse in the interstitial space and are excreted by the kidneys [57]. In plasma solution, MS-325 has a T1 relaxivity five-six times higher than extracellular/interstitial CM, while hepatospecific CM have T1 relaxivity nearly twice the relaxivity of extracellular/interstitial CM; the higher relaxivity results in a lower administered dose, in particular for Gd-EOB-DTPA and MS-325 [43–45, 56].

Extracellular/interstitial CM: pharmacokinetics and administration: Extracellular/interstitial CM (Gd-DTPA, Gd-DTPA-BMA, Gd-DTPA-BMEA, Gd-DOTA, Gd-HP-DO3A, and Gd-BT-DO3A) are small hydrophilic molecules (~500 Da) designed not to bind to plasma proteins. After intravenous injection, these CM have an early vascular phase depicting the arterial vascular anatomy. Once the CM reaches the capillary bed, they rapidly diffuse from the vascular compartment to the interstitial/extracellular space. This type of CM does not diffuse across the intact blood-brain barrier and has a very short half-life (less than 2 hours, table I) due to rapid glomerular filtration without any detectable biotransformation or metabolism. In physiological conditions and normal renal function, 98% of the administered CM is excreted within 24 hours. In the case of impaired renal function, CM

have increased half-life with increased risk of dissociation of free Gd^{3+} (dependent on the structure of chelating complexes) and deposition in several tissues [41, 57–59].

Gd-BT-DO3A is commercially available at concentration of 1 mmol[Gd]/mL, while the other five extracellular/interstitial CM are available at the concentration of 0.5 mmol[Gd]/mL [50, 60]. The FDA-approved dose is 0.1 mmol[Gd]/kg resulting in 0.1 mL/kg body weight for Gd-BT-DO3A and 0.2 mL/kg body weight for the other five extracellular/interstitial CM (table I) [50, 60]. The optimal intravenous infusion is performed with an automatic injector (injection rate ~2–3 mL/s) and is followed by a saline flush of 15–30 mL [61, 62].

Hepatospecific CM: Gd-BOPTA and Gd-EOB-DTPA

Gd-BOPTA: Gd-BOPTA has a linear, ionic framework derived from Gd-DTPA with the addition of a benzoylmethyl moiety, which allows hepatocellular uptake [63].

After intravenous infusion, Gd-BOPTA has similar kinetics as extracellular/interstitial CM, with an early vascular phase and rapid diffusion outside the vascular compartment to the extracellular/interstitial space. As other extracellular/interstitial CM, it does not cross the intact blood-brain barrier. In normal subject, the excretion is mainly via glomerular filtration, while 3–5% of the administered quantity is actively taken up by hepatocytes, with subsequent biliary excretion (see table I) [63, 64]. This proportion may change in case of impaired renal or hepatic function with compensation by the other excretion system [65]. Gd-BOPTA hepatic metabolism has been studied in animal models. Rat hepatocytes actively take up Gd-BOPTA from sinusoids via organic anion transporter proteins (OATP: rOATP1A1, rOATP1A4, and rOATP1B2) while excretion in biliary canaliculi involves multidrug resistance proteins (rMRP2). A small retrograde efflux in sinusoids has been described [66].

Gd-BOPTA shows a weak protein binding in plasma and within the hepatocyte resulting in higher relaxivity (see table I). In comparison with extracellular/interstitial CM, Gd-BOPTA has a relaxivity slightly less than twice in plasma and ~6 times higher within hepatocytes [64, 67]. This explains the high signal produced by the relatively small amount of contrast within the hepatocytes in the hepatospecific phase.

Gd-BOPTA is characterized by a distribution similar to Gd-DTPA within the first 5 min, rendering it suitable for the acquisition of vascular phases, while the maximum liver enhancement due to hepatic uptake is achieved at 60 min. The hepatospecific phase is acquired between 60 and 120 min [64, 68]. Gd-BOPTA is available in a concentration of 0.5 mmol[Gd]/mL, and the FDA recommends a dose of 0.1 mmol[Gd]/kg, resulting in 0.2 mL/Kg body weight (table I) [60]. The FDA has approved Gd-BOPTA for imaging of the central nervous system, and liver imaging is “off-label”. The injection technique is similar to extracellular/interstitial CM [61].

Gd-EOB-DTPA: Gd-EOB-DTPA is derived from Gd-DTPA with the addition of an ethoxybenzyl moiety [69]. Gd-EOB-DTPA has some peculiarities with regards to pharmacokinetics. After intravenous injection, it has weak protein binding with plasma

proteins (~10%), resulting in higher relaxivity than extracellular/interstitial CM [70]. As per Gd-BOPTA and extracellular/interstitial CM, Gd-EOB-DTPA diffuses in the extracellular/interstitial compartment and does not cross the intact blood-brain barrier [69]. Gd-EOB-DTPA is excreted to about 50% by glomerular filtration and 50% by hepatobiliary excretion, respectively (table I) [69, 71].

Hepatocytes actively uptake Gd-EOB-DTPA from sinusoids via OATP1B1 and OATP1B3, while MRP proteins are involved in the efflux of Gd-EOB-DTPA from the hepatocytes. In particular, MRP2 is expressed on the canalicular side and transports Gd-EOB-DTPA from the hepatocytes to the biliary canaliculi, while MRP3 is expressed on the sinusoidal side. The expression of MRP3 in liver parenchyma is low, and may increase in hepatocellular carcinoma or in cholestasis; retrograde efflux of Gd-EOB-DTPA is not demonstrated in physiological conditions [66, 72]. Several drugs and endogenous substances interfere with Gd-EOB-DTPA because of a common hepatic excretion pathway; in particular in case of hyperbilirubinemia (≥2mg/dL) the hepatobiliary excretion is significantly reduced [60, 66].

As per Gd-BOPTA, the weak protein binding in the hepatocellular cytoplasm increases relaxivity of Gd-EOB-DTPA, being approximately three times higher than extracellular/interstitial CM [64].

An important difference to Gd-BOPTA is the earlier hepatocellular uptake, starting at 35–40s after injection in case of Gd-EOB-DTPA vs. nearly 40 min for Gd-BOPTA (see also the shorter excretion half life in table I) [67, 73]. This aspect has an important clinical consequence: at 3–5 min the enhancement of the hepatic parenchyma is significantly influenced by the hepatic uptake of Gd-EOB-DTPA, and it is not possible to acquire a late venous phase that is substituted by a so called “transitional phase” [67, 74]. Gd-EOB-DTPA is commercially available at a concentration of 0.25 mmol[Gd]/ml, and the FDA has approved a dose of 0.025 mmol[Gd]/kg body weight, equal to 0.1 ml/kg [44].

Blood pool CM: MS-325 is the only blood pool agent in commerce, and is characterized by a transient strong protein binding. After intravenous injection, a fraction of MS-325 up to 96% binds to serum albumin, the bound fraction being inversely proportional to the CM concentration [75, 76]. The unbound fraction diffuses from the vascular compartment to the extracellular/interstitial space and is excreted mainly by glomerular filtration [39]. Unlike extracellular/interstitial CM, the serum concentration of MS-325 is high and almost constant until 60 min after injection, while, for example, only 36% of Gd-DTPA remains in the vascular compartment after 1 min and it is virtually absent in the vascular compartment at 60 min [76]. The protein binding increases the relaxivity of MS-325 in comparison with extracellular/interstitial CM, allowing a lower administered dose [60, 77]. This particular pharmacokinetics makes MS-325 suitable for vascular studies, and in liver imaging is not routinely used. Nevertheless, some authors proposed the administration of MS-325 in association with Gd-EOB-DTPA [78].

The FDA approved dose of MS-325 is 0.03 mmol/kg at low injection rate (bolus delivered in 25–30 s), followed by a saline flush [45, 57].

Superparamagnetic CM: Iron Oxides—Ferumoxytol (Feraheme, AMAG Pharmaceuticals, Cambridge, MA) is an ultrasmall superparamagnetic iron oxide (USPIO), approved for therapy of anemias [79, 80].

The molecular structure consists of iron oxide nanoparticles surrounded by a carbohydrate coating, resulting in a large molecular size and a high molecular weight (750 kDa). After intravenous injection, ferumoxytol behaves as a blood-pool agent and remains in the intravascular compartment for several hours with a long elimination half life (14–15 hours), with little vascular leakage and renal clearance. It is cleared gradually by circulating macrophages and stored in the reticuloendothelial system (RES, in liver, spleen and bone marrow) [81]. Liver clearance of ferumoxytol lasts several months [82].

Its superparamagnetic properties result in high T1, T2 and T2* relaxivity, causing strong enhancement in T1 weighted images and susceptibility effects [83].

Ferumoxitol has demonstrated an adverse events rate of about 5%, including nausea, dizziness and diarrhea, with more rare severe events. Small studies demonstrated birth defects on animals, but human data are not available. Thus Ferumoxytol should not be administered during pregnancy. The safety profile in breast feeding women is unknown. Since it has been evaluated mostly in patients with renal dysfunction, ferumoxytol may be a substitute of Gd-based CM in this category of patients. Ferumoxitol is not routinely used in liver MRI. Possible applications are vascular studies, due to the vascular kinetics, and liver imaging because of uptake by reticuloendothelial system. There is no agreement yet about the dose and the injection rates to be administered for MR studies [81].

Conclusions

MRI is a fundamental technique for the study of the liver. This technique presents several technical issues, briefly reviewed in this paper. A study of the liver cannot overlook the administration of CM: we provided the basic information on the contrast materials commercially available.

References

1. Ramalho M, Altun E, Herédia V, Zapparoli M, Semelka R. Liver MR Imaging: 1.5T versus 3T. Magnetic resonance imaging clinics of North America. 2007; 15:321–347. [PubMed: 17893053]
2. Edelstein WA, Glover GH, Hardy CJ, Redington RW. The intrinsic signal-to-noise ratio in NMR imaging. Magnetic resonance in medicine. 1986; 3:604–618. [PubMed: 3747821]
3. Soher BJ, Dale BM, Merkle EM. A review of MR physics: 3T versus 1.5T. Magnetic resonance imaging clinics of North America. 2007; 15:277–290. v. [PubMed: 17893049]
4. Busse RF. Reduced RF power without blurring: Correcting for modulation of refocusing flip angle in FSE sequences. Magnetic resonance in medicine. 2004; 51:1031–1037. [PubMed: 15122687]
5. Hargreaves BA, Cunningham CH, Nishimura DG, Conolly SM. Variable-rate selective excitation for rapid MRI sequences. Magnetic resonance in medicine. 2004; 52:590–597. [PubMed: 15334579]
6. Stanisz GJ, Odrobina EE, Pun J, et al. T1, T2 relaxation and magnetization transfer in tissue at 3T. Magnetic resonance in medicine. 2005; 54:507–512. [PubMed: 16086319]
7. Rakow-Penner R, Daniel B, Yu H, Sawyer-Glover A, Glover GH. Relaxation times of breast tissue at 1.5T and 3T measured using IDEAL. Journal of magnetic resonance imaging: JMRI. 2006; 23:87–91. [PubMed: 16315211]

8. Isoda H, Kataoka M, Maetani Y, et al. MRCP imaging at 3.0 T vs. 1.5 T: Preliminary experience in healthy volunteers. Journal of Magnetic Resonance Imaging. 2007; 25:1000–1006. [PubMed: 17410562]
9. Rohrer M, Bauer H, Mintorovitch J, Requardt M, Weinmann HJ. Comparison of magnetic properties of MRI contrast media solutions at different magnetic field strengths. Investigative radiology. 2005; 40:715–724. [PubMed: 16230904]
10. Chang KJ, Kamel IR, Macura KJ, Bluemke DA. 3.0-T MR Imaging of the Abdomen: Comparison with 1.5 T. Radiographics: a review publication of the Radiological Society of North America, Inc. 2008; 28:1983–1998.
11. Franklin KM, Dale BM, Merkle EM. Improvement in B1-inhomogeneity artifacts in the abdomen at 3T MR imaging using a radiofrequency cushion. Journal of magnetic resonance imaging: JMRI. 2008; 27:1443–1447. [PubMed: 18421685]
12. Larkman DJ, Nunes RG. Parallel magnetic resonance imaging. Physics in medicine and biology. 2007; 52:R15–55. [PubMed: 17374908]
13. Deshmane A, Gulani V, Griswold MA, Seiberlich N. Parallel MR imaging. Journal of magnetic resonance imaging: JMRI. 2012; 36:55–72. [PubMed: 22696125]
14. Pruessmann KP, Weiger M, Scheidegger MB, Boesiger P. SENSE: sensitivity encoding for fast MRI. Magnetic resonance in medicine. 1999; 42:952–962. [PubMed: 10542355]
15. Sodickson DK, Manning WJ. Simultaneous acquisition of spatial harmonics (SMASH): Fast imaging with radiofrequency coil arrays. Magnetic resonance in medicine. 1997; 38:591–603. [PubMed: 9324327]
16. Jakob PM, Griswold MA, Edelman RR, Sodickson DK. AUTO-SMASH: a self-calibrating technique for SMASH imaging. SiMultaneous Acquisition of Spatial Harmonics. Magma (New York, NY). 1998; 7:42–54.
17. Heidemann RM, Griswold MA, Haase A, Jakob PM. VD-AUTO-SMASH imaging. Magnetic resonance in medicine. 2001; 45:1066–1074. [PubMed: 11378885]
18. Griswold MA, Jakob PM, Heidemann RM, et al. Generalized autocalibrating partially parallel acquisitions (GRAPPA). Magnetic resonance in medicine. 2002; 47:1202–1210. [PubMed: 12111967]
19. Breuer FA, Blaimer M, Heidemann RM, Mueller MF, Griswold MA, Jakob PM. Controlled aliasing in parallel imaging results in higher acceleration (CAIPIRINHA) for multi-slice imaging. Magnetic resonance in medicine. 2005; 53:684–691. [PubMed: 15723404]
20. Pruessmann KP. Parallel imaging at high field strength: synergies and joint potential. Topics in magnetic resonance imaging: TMRI. 2004; 15:237–244. [PubMed: 15548954]
21. Wood ML, Henkelman RM. MR image artifacts from periodic motion. Medical physics. 1985; 12:143–151. [PubMed: 4000069]
22. Zaitsev M, Maclaren J, Herbst M. Motion artifacts in MRI: A complex problem with many partial solutions. Journal of magnetic resonance imaging: JMRI. 2015; 42:887–901. [PubMed: 25630632]
23. Wade OL. Movements of the thoracic cage and diaphragm in respiration. The Journal of Physiology. 1954; 124:193–212. [PubMed: 13175123]
24. Bernstein, MA.King, KF., Zhou, XJ., editors. Handbook of MRI Pulse Sequences. Elsevier Science; 2004. Basics of physiologic gating, triggering, and monitoring.
25. Guglielmo FF, Mitchell DG, Roth CG, Deshmukh S. Hepatic MR Imaging Techniques, Optimization, and Artifacts. Magnetic Resonance Imaging Clinics. 2014; 22:263–282.
26. Lewis CE, Prato FS, Drost DJ, Nicholson RL. Comparison of respiratory triggering and gating techniques for the removal of respiratory artifacts in MR imaging. Radiology. 1986; 160:803–810. [PubMed: 3737921]
27. Bailes DR, Gilderdale DJ, Bydder GM, Collins AG, Firmin DN. Respiratory ordered phase encoding (ROPE): a method for reducing respiratory motion artefacts in MR imaging. Journal of computer assisted tomography. 1985; 9:835–838. [PubMed: 4019854]
28. Hargreaves BA. Rapid gradient-echo imaging. Journal of magnetic resonance imaging: JMRI. 2012; 36:1300–1313. [PubMed: 23097185]
29. Ichikawa T, Araki T. Fast magnetic resonance imaging of liver. European journal of radiology. 1999; 29:186–210. [PubMed: 10399607]

30. Scheffler K, Lehnhardt S. Principles and applications of balanced SSFP techniques. European radiology. 2003; 13:2409–2418. [PubMed: 12928954]
31. Bayramoglu S, Kilickesmez O, Cimilli T, et al. T2-weighted MRI of the upper abdomen: comparison of four fat-suppressed T2-weighted sequences including PROPELLER (BLADE) technique. Acad Radiol. 2010; 17:368–374. [PubMed: 20042352]
32. Pipe JG. Motion correction with PROPELLER MRI: application to head motion and free-breathing cardiac imaging. Magnetic resonance in medicine. 1999; 42:963–969. [PubMed: 10542356]
33. Korin HW, Felmlee JP, Ehman RL, Riederer SJ. Adaptive technique for three-dimensional MR imaging of moving structures. Radiology. 1990; 177:217–221. [PubMed: 2399320]
34. Nagle SK, Busse RF, Brau AC, et al. High Resolution Navigated 3D T(1)-weighted Hepatobiliary MRI using Gadoxetic Acid Optimized for 1.5T. Journal of magnetic resonance imaging: JMRI. 2012; 36:890–899. [PubMed: 22648633]
35. Klessen C, Asbach P, Kroencke TJ, et al. Magnetic resonance imaging of the upper abdomen using a free-breathing T2-weighted turbo spin echo sequence with navigator triggered prospective acquisition correction. Journal of magnetic resonance imaging: JMRI. 2005; 21:576–582. [PubMed: 15834908]
36. Vasanawala SS, Iwadate Y, Church DG, Herfkens RJ, Brau AC. Navigated abdominal T1-W MRI permits free-breathing image acquisition with less motion artifact. Pediatric Radiology. 2010; 40:340–344. [PubMed: 20066407]
37. Asbach P, Warmuth C, Stemmer A, et al. High spatial resolution T1-weighted MR imaging of liver and biliary tract during uptake phase of a hepatocyte-specific contrast medium. Investigative radiology. 2008; 43:809–815. [PubMed: 18923261]
38. Wood ML, Hardy PA. Proton relaxation enhancement. Journal of magnetic resonance imaging: JMRI. 1993; 3:149–156. [PubMed: 8428082]
39. Hao D, Ai T, Goerner F, Hu X, Runge VM, Tweedle M. MRI contrast agents: basic chemistry and safety. Journal of magnetic resonance imaging: JMRI. 2012; 36:1060–1071. [PubMed: 23090917]
40. Haley TJ, Raymond K, Komesu N, Upham HC. Toxicological and pharmacological effects of gadolinium and samarium chlorides. British journal of pharmacology and chemotherapy. 1961; 17:526–532. [PubMed: 13903826]
41. Thomsen HS, Morcos SK, Almen T, et al. Nephrogenic systemic fibrosis and gadolinium-based contrast media: updated ESUR Contrast Medium Safety Committee guidelines. European radiology. 2013; 23:307–318. [PubMed: 22865271]
42. Food and Drug Administration. MAGNEVIST (gadopentetate dimeglumine). 2013. http://www.accessdata.fda.gov/drugsatfda_docs/label/2013/019596s056,021037s029lbl.pdf
43. Food and Drug Administration. MultiHance. 2010. http://www.accessdata.fda.gov/drugsatfda_docs/label/2010/021357s009lbl.pdf
44. Food and Drug Administration. EOVIST (Gadoxetate Disodium). 2010. http://www.accessdata.fda.gov/drugsatfda_docs/label/2010/022090s004lbl.pdf
45. Food and Drug Administration. ABLAVAR (gadofosveset trisodium). 2010. http://www.accessdata.fda.gov/drugsatfda_docs/label/2009/022180lbl.pdf
46. Food and Drug Administration. OMNISCAN (gadodiamide). 2010. http://www.accessdata.fda.gov/drugsatfda_docs/label/2010/020123s037lbl.pdf
47. Food and Drug Administration. OptiMARK (gadoversetamide. 2013. http://www.accessdata.fda.gov/drugsatfda_docs/label/2013/020937s021,020975s022,020976s022lbl.pdf
48. Food and Drug Administration. DOTAREM (gadoterate meglumine). 2013. http://www.accessdata.fda.gov/drugsatfda_docs/label/2013/204781s000lbl.pdf
49. Food and Drug Administration. ProHance (Gadoteridol). 2010. http://www.accessdata.fda.gov/drugsatfda_docs/label/2010/020131s024lbl.pdf
50. Food and Drug Administration. Gadavist (gadobutrol). 2013. http://www.accessdata.fda.gov/drugsatfda_docs/label/2013/201277s003lbl.pdf
51. Caravan P, Ellison JJ, McMurry TJ, Lauffer RB. Gadolinium(III) Chelates as MRI Contrast Agents: Structure, Dynamics, and Applications. Chemical Reviews. 1999; 99:2293–2352. [PubMed: 11749483]

52. Morcos SK. Nephrogenic systemic fibrosis following the administration of extracellular gadolinium based contrast agents: is the stability of the contrast agent molecule an important factor in the pathogenesis of this condition? Br J Radiol. 2007; 80:73–76. [PubMed: 17392401]
53. De Leon-Rodriguez LM, Martins AF, Pinho MC, Rofsky NM, Sherry AD. Basic MR relaxation mechanisms and contrast agent design. Journal of magnetic resonance imaging: JMRI. 2015; 42:545–565. [PubMed: 25975847]
54. Frenzel T, Lengsfeld P, Schirmer H, Hutter J, Weinmann HJ. Stability of gadolinium-based magnetic resonance imaging contrast agents in human serum at 37 degrees C. Investigative radiology. 2008; 43:817–828. [PubMed: 19002053]
55. American college of Radiology – ACR Committee on Drugs and Contrast Media. ACR Manual on Contrast Media – Version 10.1. 2015. http://www.acr.org/~/media/ACR/Documents/PDF/QualitySafety/Resources/Contrast%20Manual/2015_Contrast_Media.pdf
56. Cavagna FM, Maggioni F, Castelli PM, et al. Gadolinium chelates with weak binding to serum proteins. A new class of high-efficiency, general purpose contrast agents for magnetic resonance imaging. Investigative radiology. 1997; 32:780–796. [PubMed: 9406019]
57. Bellin MF, Van Der Molen AJ. Extracellular gadolinium-based contrast media: an overview. European journal of radiology. 2008; 66:160–167. [PubMed: 18358659]
58. Tweedle MF, Wedeking P, Kumar K. Biodistribution of radiolabeled, formulated gadopentetate, gadoteridol, gadoterate, and gadodiamide in mice and rats. Investigative radiology. 1995; 30:372–380. [PubMed: 7490190]
59. Oksendal AN, Hals P-A. Biodistribution and toxicity of MR imaging contrast media. Journal of Magnetic Resonance Imaging. 1993; 3:157–165. [PubMed: 8428083]
60. Guglielmo FF, Mitchell DG, Gupta S. Gadolinium contrast agent selection and optimal use for body MR imaging. Radiologic clinics of North America. 2014; 52:637–656. [PubMed: 24889165]
61. Earls JP, Rofsky NM, DeCorato DR, Krinsky GA, Weinreb JC. Hepatic arterial-phase dynamic gadolinium-enhanced MR imaging: optimization with a test examination and a power injector. Radiology. 1997; 202:268–273. [PubMed: 8988222]
62. Van Beers BE, Materne R, Lacrosse M, et al. MR imaging of hypervascular liver tumors: timing optimization during the arterial phase. Journal of magnetic resonance imaging: JMRI. 1999; 9:562–567. [PubMed: 10232515]
63. Cheng, KT. Molecular Imaging and Contrast Agent Database (MICAD). Bethesda (MD): National Center for Biotechnology Information (US); 2004. Gadobenate.
64. Kirchin MA, Pirovano GP, Spinazzi A. Gadobenate dimeglumine (Gd-BOPTA). An overview. Investigative radiology. 1998; 33:798–809. [PubMed: 9818314]
65. Kirchin MA, Lorusso V, Pirovano G. Compensatory biliary and urinary excretion of gadobenate ion after administration of gadobenate dimeglumine (MultiHance®) in cases of impaired hepatic or renal function: a mechanism that may aid in the prevention of nephrogenic systemic fibrosis? The British Journal of Radiology. 2015; 88:20140526. [PubMed: 25651409]
66. Pastor CM, Mullhaupt B, Stieger B. The role of organic anion transporters in diagnosing liver diseases by magnetic resonance imaging. Drug metabolism and disposition: the biological fate of chemicals. 2014; 42:675–684. [PubMed: 24398460]
67. Giovagnoni A, Paci E. Liver. III: Gadolinium-based hepatobiliary contrast agents (Gd-EOB-DTPA and Gd-BOPTA/Dimeg). Magnetic resonance imaging clinics of North America. 1996; 4:61–72. [PubMed: 8673717]
68. Planchamp C, Gex-Fabry M, Dornier C, et al. Gd-BOPTA transport into rat hepatocytes: pharmacokinetic analysis of dynamic magnetic resonance images using a hollow-fiber bioreactor. Investigative radiology. 2004; 39:506–515. [PubMed: 15257212]
69. Cheng, KT. Molecular Imaging and Contrast Agent Database (MICAD). Bethesda (MD): National Center for Biotechnology Information (US); 2004. Gadoxetate.
70. Reimer P, Schneider G, Schima W. Hepatobiliary contrast agents for contrast-enhanced MRI of the liver: properties, clinical development and applications. European radiology. 2004; 14:559–578. [PubMed: 14986050]

71. Hamm B, Staks T, Muhler A, et al. Phase I clinical evaluation of Gd-EOB-DTPA as a hepatobiliary MR contrast agent: safety, pharmacokinetics, and MR imaging. Radiology. 1995; 195:785–792. [PubMed: 7754011]
72. Vilgrain V, Van Beers BE, Pastor CM. Insights into the diagnosis of hepatocellular carcinomas with hepatobiliary MRI. J Hepatol. 2015
73. Schalkx HJ, van Stralen M, Coenegrachts K, et al. Liver perfusion in dynamic contrast-enhanced magnetic resonance imaging (DCE-MRI): comparison of enhancement in Gd-BT-DO3A and Gd-EOB-DTPA in normal liver parenchyma. European radiology. 2014; 24:2146–2156. [PubMed: 24996795]
74. American College of Radiology (ACR). Liver Reporting and Data System (LIRADS). 2014. https://nrdr.acr.org/lirads/
75. Lauffer RB, Parmelee DJ, Dunham SU, et al. MS-325: albumin-targeted contrast agent for MR angiography. Radiology. 1998; 207:529–538. [PubMed: 9577506]
76. Farooki A, Narra V, Brown J. Gadofosveset (EPIX/Schering). Current opinion in investigational drugs (London, England: 2000). 2004; 5:967–976.
77. Eldredge HB, Spiller M, Chasse JM, Greenwood MT, Caravan P. Species dependence on plasma protein binding and relaxivity of the gadolinium-based MRI contrast agent MS-325. Investigative radiology. 2006; 41:229–243. [PubMed: 16481905]
78. Bannas P, Motosugi U, Hernando D, Rahimi MS, Holmes JH, Reeder SB. Combined gadoxetic acid and gadofosveset enhanced liver MRI: A feasibility and parameter optimization study. Magnetic resonance in medicine. 2016; 75:318–328. [PubMed: 25648403]
79. Bashir MR. Magnetic resonance contrast agents for liver imaging. Magnetic resonance imaging clinics of North America. 2014; 22:283–293. [PubMed: 25086930]
80. Food and Drug Administration. Feraheme™ (ferumoxytol). 2009. http://www.accessdata.fda.gov/drugsatfda_docs/label/2009/022180lbl.pdf
81. Bashir MR, Bhatti L, Marin D, Nelson RC. Emerging applications for ferumoxytol as a contrast agent in MRI. Journal of Magnetic Resonance Imaging. 2015; 41:884–898. [PubMed: 24974785]
82. Storey P, Lim RP, Chandarana H, et al. MRI assessment of hepatic iron clearance rates after USPIO administration in healthy adults. Investigative radiology. 2012; 47:717–724. [PubMed: 23070094]
83. Corot C, Robert P, Idée J-M, Port M. Recent advances in iron oxide nanocrystal technology for medical imaging. Advanced Drug Delivery Reviews. 2006; 58:1471–1504. [PubMed: 17116343]

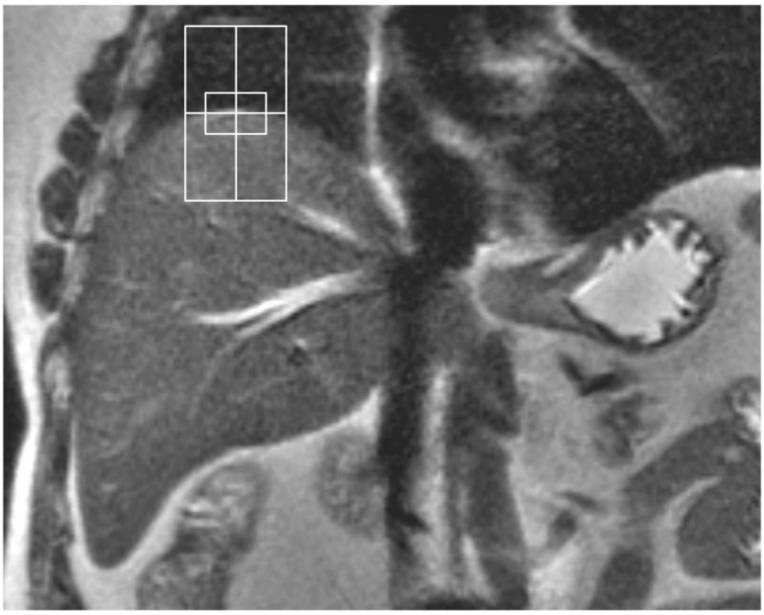

Figure 1. Navigator

Coronal T2-weighted SSFSE demonstrating correct positioning of bidimensional navigator. The center of the navigator is positioned tangent to the dome of the right hemidiaphragm.

Table I

Overview of FDA approved contrast materials

FDA approved nine different contrast materials. In this table they are ordered following the ESUR guidelines for patients at risk of NSF, and compared with ACR groups for related cases of NSF.

ESUR	ACR	Structure		Contrast		Concentration	Dose	R1 Plasma, 37°C		Distribution	Protein binding	Elimination		Dissociation
NSF RISK	NSF GROUP			Name	Brand Name	mmol/mL	mmol/kg (mL/kg)	1.5T	3T			Clearance	T_e1/2 (hrs)	T_d1/2 pH=1
LOW	2	Macro-cyclic	Ionic	**Gd-DOTA** (Gadoterate meglumine)	Dotarem/Magnescope	0.5	0.1 (0.2)	3.6	3.5	Extracellular	No	Renal	1.6±0.2 *(mono)*	9–229 hrs
			Non ionic	**Gd-HP-DO3A** (Gadoteridol)	ProHance	0.5	0.1 (0.2)	4.1	3.7	Extracellular	No	Renal	0.20±0.04; 1.57±0.08 (*bi*)	3 hrs
				Gd-BT-DO3A (Gadobutrol)	Gadovist/Gadavist	1	0.1 (0.1)	5.2	5	Extracellular	No	Renal	1.81	68 hrs
INTERMEDIATE	2	Linear	Ionic	**Gd-BOPTA** (Gadobenate dimeglumine)	MultiHance	0.5	0.1 (0.2)	6.3	5.5	Extracellular - Liver	Weak	Renal ~95% Hepatic 3–5%	1.17±0.26 – 2.02±0.60 *(range)*	-
	3			**Gd-EOB-DTPA** (Gadoxetate disodium)	Primovist/Eovist	0.25	0.025 (0.1)	6.9	6.2	Extracellular - Liver	Weak	Renal 50% Hepatic 50%	0.91–0.95 *(range)*	-
				MS-325 (Gadofosveset trisodium)	Vasovist/Ablavar	0.25	0.03 (0.12)	19	9.9	Blood pool	Strong	Renal 79–94% Hepatic~5%	16.3±2.6	-
HIGH	1			**Gd-DTPA** (Gadopentetate dimeglumine)	Magnevist	0.5	0.1 (0.2)	4.1	3.7	Extracellular	No	Renal	1.6±0.16	9.6 min
			Non Ionic	**Gd-DTPA-BMEA** (Gadoverse tamide)	Optimark	0.5	0.1 (0.2)	4.7	4.5	Extracellular	No	Renal	1.73±0.33	-
				Gd-DTPA-BMA (Gadodiamide)	Omniscan	0.5	0.1 (0.2)	4.3	4.0	Extracellular	No	Renal	0.06±0.05; 1.30±0.27 *(bi)*	<34 s

ESUR: European Society of Urogenital Radiology. **ACR:** American College of Radiology. **NSF:** Nephrogenic Systemic Fibrosis. **R1:** Relaxivity R1 at 1.5T and 3T, in plasma at 37°C. **T_e1/2:** excretion half-life. **T_d1/2:** Gadolinium-chelating compound dissociation half-life, calculated at pH=1. **mono:** monocompartmental model. **bi:** bicompartmental model. **hrs:** hours. **min:** minutes. **s:** seconds.